# Towards a Remote Inspection of Jet Engine Blades Using Time Reversal

Maxime Farin[a], Claire Prada[a], Tony Lhommeau[b], Mohammed El Badaoui[c], Julien de Rosny[a,*]

[a]*Institut Langevin, ESPCI Paris, Université PSL, CNRS, 75005 Paris, France*
[b]*Safran Aircraft Engines, Rond Point René Ravaud - Réau, Moissy-Cramayel, France*
[c]*SafranTech, Rue des Jeunes Bois - Châteaufort, Magny-les-Hameaux, France*

## Abstract

Assessing the state of damage of jet engine blades is a burning issue in aeronautics. However, most nondestructive evaluation procedures require cumbersome installations and removal of the blades from the engines, which is time and money consuming. We present a non-intrusive acoustic monitoring technique that could be applied for fast remote inspection of selected blades inside a jet engine. The technique uses a time reversal mirror in the audible frequency range to selectively excite a targeted blade a few meters away. The resonance frequencies of the blade are measured at the location of the excitation using a laser vibrometer. The technique is first applied on a few individual blades and then inside a jet engine. Selective excitation of a difficult-to-access blade among others inside a cavity is shown. In laboratory, some damage (material removal or slit) is created on a set of initially intact blades, which cause a shift in their resonance frequencies. By evaluating these frequency shifts, we are able to remotely detect millimeter size damage on the blades. Finally, the on-site applicability and the uncertainties of the method are discussed.

*Keywords:* nondestructive evaluation, time reversal, blades
*PACS:* 43.60.Tj, 43.40.Le, 43.40.Dx

## 1. Introduction

Solid thin plates, shells and pipes are used in various industrial domains (e.g., aeronautics, automobile, food-processing, wind energy, ...). Numerous monitoring techniques are routinely applied to detect and localize damage

*julien.derosny@espci.psl.eu
*Email address:* julien.derosny@espci.psl.eu (Julien de Rosny)

such as fatigue cracks, corrosion or delamination on these structures [see 1, 2, for review]. Optical control goes from simple naked eyes inspection to tracking changes in the material light transmission due to stress that accumulate around the damage. Ultrasonic scans provide precise location and size estimate of damage but can require the operator to place the investigated object in a bath of water or into a dye penetrant solution that can affect the materials properties, as well as being expensive to conduct [e.g., 3, 4]. Complementary to optical methods, acoustic nondestructive testing (NDT) methods such as the coin-tap method [5] or resonant ultrasound spectroscopy (RUS) [6] consist in tracking changes in the eigenfrequencies of solids to probe their structural properties and to detect and characterize damage [e.g. 7, 8, 9, 10]. Recent approaches detect the harmonics generated by the excitation of non-linear defects [see 11, for review]. These methods are active since they require the excitation of the investigated solid with an impact or a piezoelectric transducer to measure its frequency spectrum. In contrast, passive methods record acoustic signals produced by the damage during its growth [12], or take advantage of the ambient acoustic noise around the structure (e.g., engine noise or wind) to localize flaws [13, 14]. The problem with all of these inspection techniques is that they require complete removal of the investigated object from the structure, time expensive full scan of the object and/or involves cumbersome installation of transducers and sensors. More importantly, a direct contact with the object is needed and can be challenging to achieve.

Recently, Le Bas et al. [15, 16] and Farin et al. [17] showed that it is possible to remotely measure the frequency response of an object using a time reversal mirror (TRM). A TRM operates on a two-step procedure [see 18, for a review of pioneer time reversal (TR) papers]. In the first step (forward step), a wave is emitted by a source and recorded by a set of transducers (the TRM). In the second step (backward step), the recorded signals are flipped in time and played back by the transducers. The re-emitted waves then focus as a pulse at the initial source position. Such TRMs have been applied in various contexts such as nondestructive testing [19, 20], underwater acoustics [21] or room acoustics [22]. Le Bas et al. [15, 16] built an air-coupled TRM consisting of piezoelectric transducers enclosed inside a hollow reverberant cavity with an opening located a few centimeters above a tested plate. In the forward step, the transducers successively emit an ultrasonic wave that couples to the plate's vibration modes which are recorded at a single point on the plate using a laser vibrometer. In the backward step, the time-reversed signals are played simultaneously by all transducers to locally excite the plate. Besides the classical array effect, the focusing is enhanced by the reverberation of the sound waves inside the cavity and of the flexural waves inside the plate, as already shown by Draeger et al. [23]. Indeed, TR process is improved in complex media [24, 25, 26]. After conducting the forward step at an intact location of a laminated composite plate, Le Bas et al. [16] repeated the backward step for several locations of the cavity to provide a 2D-scan of the plate response. At certain positions, the plate response had a different amplitude and frequency than the reference at the intact location, which revealed delamination. Farin et al. [17] proposed a slightly different but complementary approach. Their TRM is composed of a network of loudspeakers operating in the audible frequency range (1-10 kHz) to remotely make thin plates vibrate and measure their eigenfrequencies. The eigenfrequencies are measured at the excitation point with a laser vibrometer. Working in the audible frequency range allows Farin et al. to selectively excite an object located a few meters away and inside a complex structure i.e., in conditions for which the object would be too difficult to access using the standard coin-tap method or other approaches using ultrasound [e.g. 16].

In this paper, we propose to apply this TR technique to control jet engine blades. Standard routine inspection of these blades requires disassembly of the engine, immobilizing the aircraft for hours. In Farin et al. [17], simple duralumin plates were excited with an array of loudspeakers. The question remained as to whether the TR technique will also be efficient for titanium blades of curved shapes and non-uniform thicknesses. Moreover, we also want to test the selective excitation of blades that are mounted on their wheel and surrounded by others inside the engine, which structure is designed to attenuate vibrations. Basically, our approach is similar to the previously mentioned RUS methods [e.g. 7, 8, 9] but with a TR excitation of the inspected objects. While our objective is not to achieve better damage detection and characterization than what was done in these studies, we would like to show that the eigenfrequencies of a blade can be measured with sufficient accuracy to remotely detect and quantify millimeter-size damage. In section 2, we present the experimental setup. In section 3, the time reversal technique is applied on several blades, first in laboratory conditions and then inside a jet engine. In section 4, we measure the effect of different damages that we created on several blades. We analyze how the observed eigenfrequency shifts are related to the damage sizes. Finally, in section 5, we discuss the uncertainties of the proposed TR technique and the on-site application.

## 2. Experimental Setup

The TRM consists of an array of 32 loudspeakers (LS) arranged on a $8 \times 4$ vertical panel with a 20 cm inter-element spacing (Fig. 1). The diameter of the LS (Ryght Y-Storm) equals 6 cm. They are connected to a homemade electronic card to amplify the signals and to a 32-channel analog-digital/digital-analog (AD/DA) converter (Orion 32 channels, Antelope) that sends and samples the data from/to the computer at a rate of 96 kS/s. We use Python and the PyAudio library to communicate with the AD/DA converter and process the emitted and received waveforms.

During the forward step of the TR procedure, a 1-s long linear frequency modulated signal between 1 kHz and 10 kHz is emitted with a loudspeaker at position $\mathbf{r_i}$ (Fig. 1a). A laser vibrometer (Polytec OFU-505) measures the resulting blade vibration at a given position $\mathbf{r_0}$. The deconvolution of the emitted chirp with recorded signals allows us to determine the impulse responses of the media $k_i(t)$ from the loudspeaker at $\mathbf{r_i}$ to position $\mathbf{r_0}$. This measurement is repeated for each LS in order to obtain the set of responses $k_i(t)$, $1 \leq i \leq 32$. (Fig. 1a). During the backward step, all LS simultaneously emit the time-reversed responses $k_i(T - t)$ (Fig. 1b). This operation maximizes the energy focused on the blade, at position $\mathbf{r_0}$ and at time $T$ from the beginning of the reemission, in order to excite its eigenmodes [17]. The two-step TR experiment conducted to record the eigenfrequencies at one position lasts about 40 seconds. The recorded impulse responses have a high signal-to-noise ratio because the excitation signals have a long duration of 1 s. Therefore, our measurements do not need to be averaged. The reverberation time necessary for the sound pressure to decreases by 60 dB in the impulse response is estimated to be about 0.74 s in the frequency range of interest (1-10 kHz). The noise level being about -25 dB with respect to the impulse response maximum (0 dB), the length of the impulse responses used for the TR focusing operation consequently lasts about 0.3 s.

## 3. Remote Excitation of Blades

First, in laboratory conditions, we verify the focusing ability at different positions on several blades and find preferential excitation positions. Then, we test the selective excitation of one blade in a set of three placed close to each other inside a complex structure. Finally, to get closer to real conditions, we deploy a similar setup in front of a jet engine.

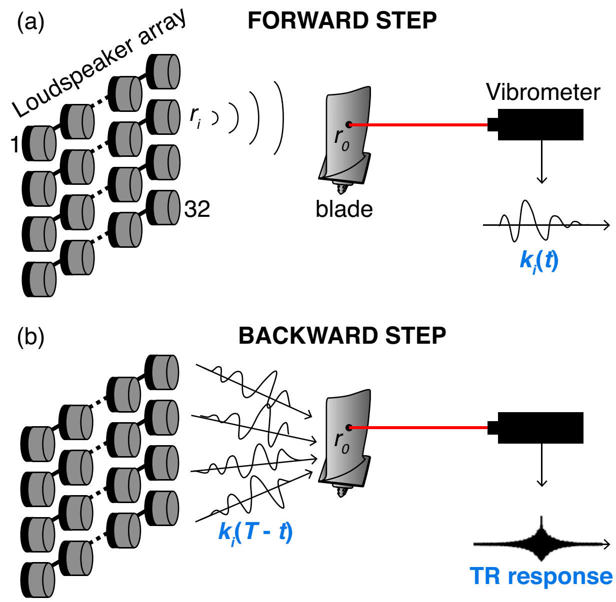


Figure 1: Schematic of the experiment. (a) During the forward step, the impulse responses $k_i(t)$ between each loudspeaker in $\mathbf{r_i}$ and a position $\mathbf{r_0}$ on the blade are recorded using a laser vibrometer. (b) During the backward step, all impulse responses are time reversed $(k_i(T-t))$ and played simultaneously and the TR response (pulse) is measured at position $\mathbf{r_0}$.

### *3.1. Laboratory Measurements on Blades*

The TR excitation technique is applied on a set of rectangular blades of three different sizes: 'small' blades of dimensions $\sim 7 \times 5.5$ cm$^2$, 'medium' blade of dimensions $\sim 16.5 \times 8.5$ cm$^2$ and 'large' blades of dimensions $\sim 21 \times 14$ cm$^2$. The blades are composed of titanium alloy and have a curved shape (as displayed on Figure 3a). They are a few millimeter thick and thinner at the top and along the edges. The blades are placed successively about one meter away from the TRM on a 1-m tall microphone stand. We record responses (pulses) after similar TR focusing processes on the three blades (Fig. 2a-c). Fig. 2d-f show an enlargement a few periods around the central pulses. The pulses focused in the blades are short in time (a few ms) and therefore we excite blade eigenmodes over a wide frequency range. Only a few eigenmodes are observed in the amplitude spectra of the pulses (Fig. 2ghi) in the frequency range of interest (1-10 kHz). More eigenmodes are detected below 10 kHz on the medium and large blades ($\sim$ 20 eigenmodes) than on the small blade ($\sim 8$ eigenmodes). For each blades, we focus a pulse

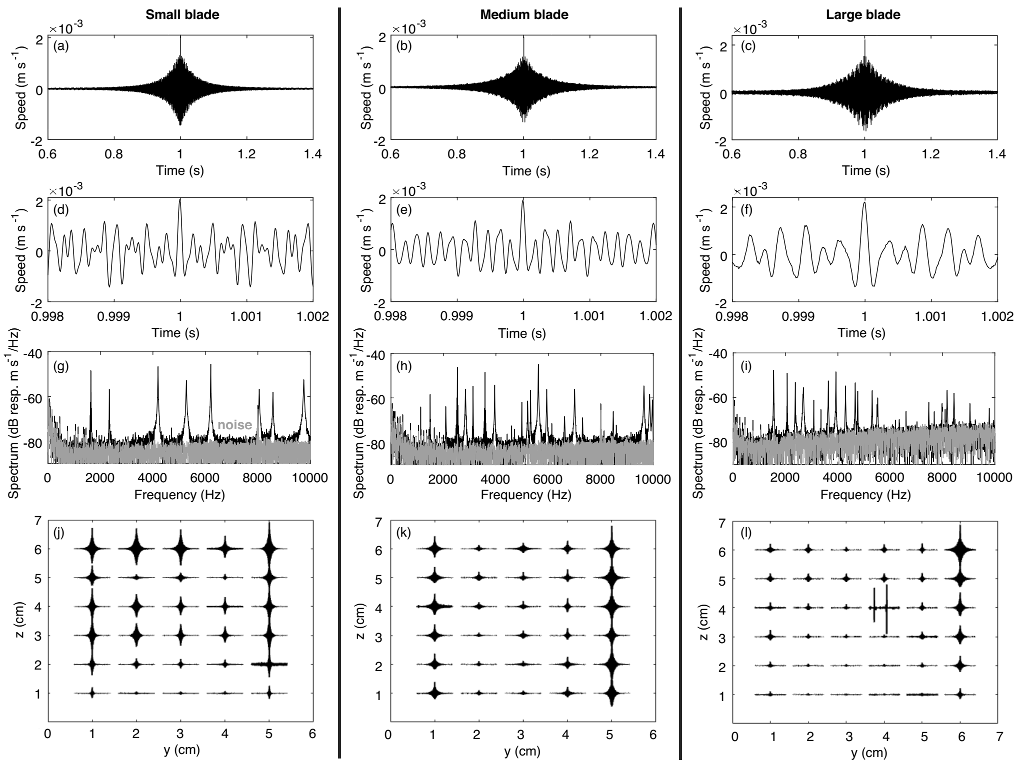


Figure 2: (a)-(c) Responses recorded after TR focusing at one point on each blade, (d)-(f) Enlargement around the pulse maximum, (g)-(i) Amplitude spectra (obtained by Fourier transform) of the pulses showed in panels (d)-(f) (black) and of a noise signal of same duration (grey) and (j)-(l) TR response at different positions for (a), (d), (g) and (j) the small blade, (b), (e), (h) and (k) the medium blade and (c), (f), (i) and (l) the large blade. Pulses amplitudes in panels (j)-(l) are normalized with respect to the amplitude of the largest pulse on each blade.

at 30 to 36 different positions (Fig. 2jkl). It is clear that the geometry of the blades affect the excitation amplitude. Indeed, the amplitude is higher along the thin edges which are more flexible, while it is lower at the center or at the thick bottom of the blade, where displacement is more constrained. On the blade edges, the focusing efficiency is at maximum 1%. This number is evaluated as the ratio of the elastic energy stored in the blade deduced from the vibrometer scan to the estimated total radiated sound power. See [17] for details on the computation of this ratio.

It is observed that the displacements are larger along the thin blade edges. This is in agreement with numerical simulations of the eigenmodes of the small blade calculated with a finite elements method using a mesh built from measurements of the blade thickness (Fig. 3ab). Elastic parameters are those of titanium. The amplitude of the excitation correlates with the local displacement of the corresponding excited eigenmodes (Fig. 3b).

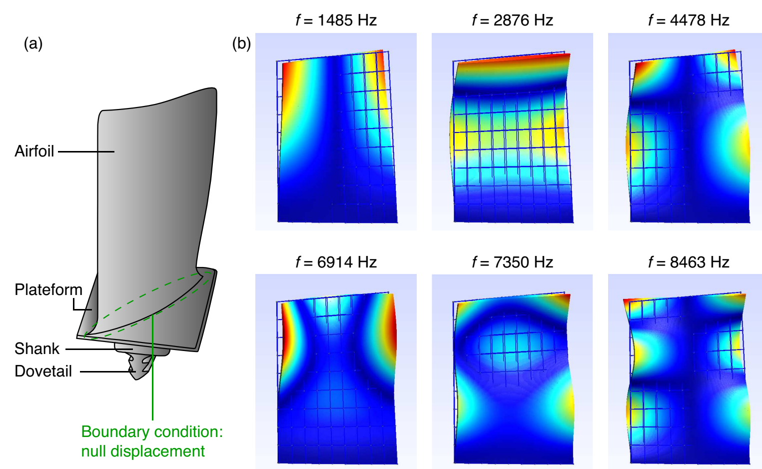


Figure 3: (a) Schematic of a blade used in the experiments. To simulate the eigenmodes using a finite elements model (GetDP, [27]), a null displacement is imposed at the bottom of the blade. (b) Different eigenmodes simulated for the small blade and their corresponding frequencies. Red indicates greater displacement.

In the next experiment, three small blades are placed side-by-side inside a PVC tube and we try to excite one of them (Fig. 4). The blades are simply supported on a 3D-printed stand. Reflecting tape is applied to the blades in order to scan them with the vibrometer and check the focusing. It appears that the TR focusing on one blade does not excite much the other blades. The ratio of the maximum vibration amplitude on the excited blade to the vibration amplitude on the two other blades varies from 2 (in the middle blade left corner) to 20 (at the bottom of the blades), with an average ratio around 15. It is noticeable that the TR focusing is effective although the central blade is partially hiding the focusing position of the selected blade from the LS array. Therefore, one can excite blades and selectively measure their eigenmodes independently of the other blades around it.

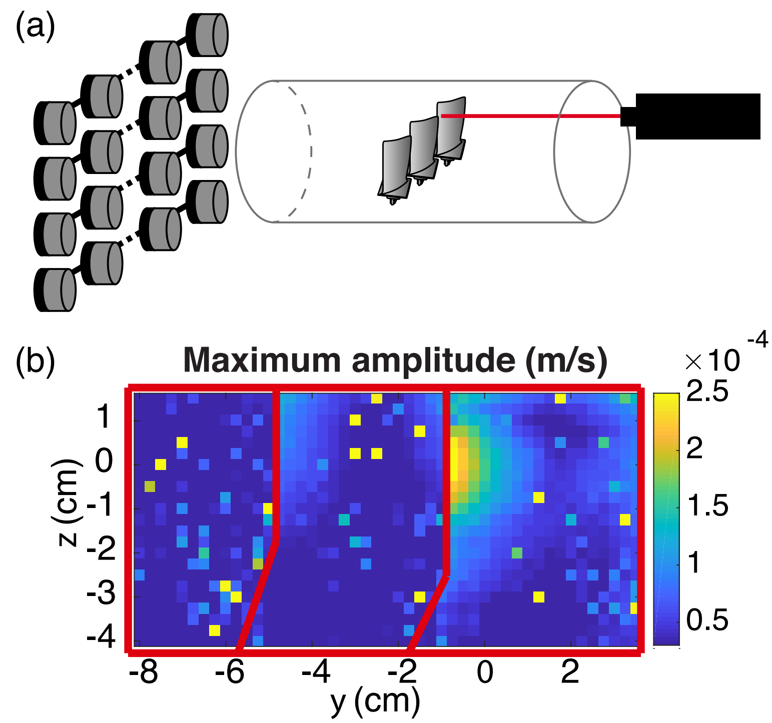


Figure 4: (a) Schematic of the three blades placed inside a PVC tube of thickness 5 mm, diameter 20 cm and length 2 m. The blades are scanned with the laser vibrometer. (b) Maximum amplitude of the unfiltered vibration signal measured by the vibrometer at each position of the blades after TR focusing at position ($y = 0, z = 0$). Red lines delimitate the three blades, which have a curved shape.

### *3.2. Excitation of Blades Inside a Jet Engine*

In order to approach real conditions, we conducted measurements on blades embedded inside a jet engine. The deployed experimental setup is simple, with a panel of 16 LS arranged in a 4-by-4 array with a 20-cm inter-element spacing and a laser vibrometer, located at the front of the engine (Fig. 5). With this setup, two types of blades are investigated: (1) the fan blades at the entrance of the engine and (2) compressor blades of the second mobile wheel, similar to the ‘small’ blades investigated in the laboratory. We also installed four microphones to verify acoustic signal transmission through the engine. Unfortunately, our loudspeakers were not powerful enough to sufficiently excite the rigid structure of the first fixed wheel of inlet guide vanes.

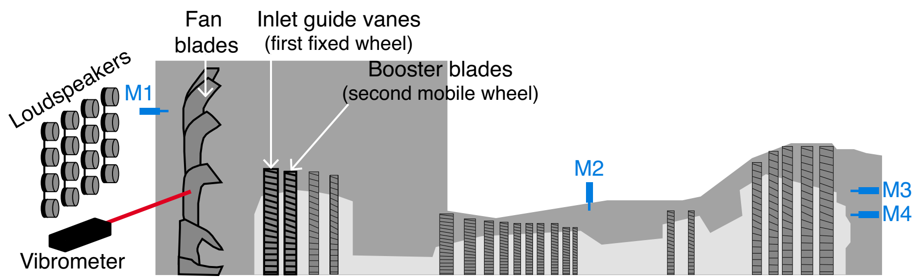


Figure 5: Simplified schematic showing the experimental setup deployed around the jet engine and the investigated blades. The TRM is a panel of 16 LS located at the front of the engine. A laser vibrometer measures the vibration of the excited blade. Four microphones are installed at the front (M1), through a side access (M2) and at the back (M3 and M4) of the engine.

#### *3.2.1. Focusing on Frontal Blades*

Because the fan-blade wheel can be rotated, we exploit the possibility to record the impulse responses during the forward step of the TR process on a given fan blade and then use these impulse responses during the backward step to focus on other fan blades successively placed at the same position after rotation of the wheel (i.e. invariance of the cavity). This simplified operation could shorten the routine inspection from about 40 seconds per blade with the standard TR experiment to about 1 s per blade if we only conduct the backward step. With this procedure, it appears that the focusing pulse and the secondary lobes are similar on the blade on which we recorded the impulse responses (black curve in Fig. 6a) to the ones recorded on the four other fan blades (colored curves in Fig. 6a). The impulse amplitude is slightly lower on the four other blades but the curves follow the same low-frequency variation on all blades. The eigenmodes of the blades are similar on the five investigated blades, especially from 1000 Hz to 3000 Hz (Fig. 6b). Discrepancy between the eigenmodes may originate from the fact that the fan blades may not be placed at the exact same position when rotating the wheel or from slight manufacturing differences from one fan blade to the other. Finally, we excite a booster blade of the second mobile wheel. The blade is partially hidden behind the fan blades and the inlet guide vanes but the focused pulse and the eigenmodes are well visible (Fig. 6ef). However,

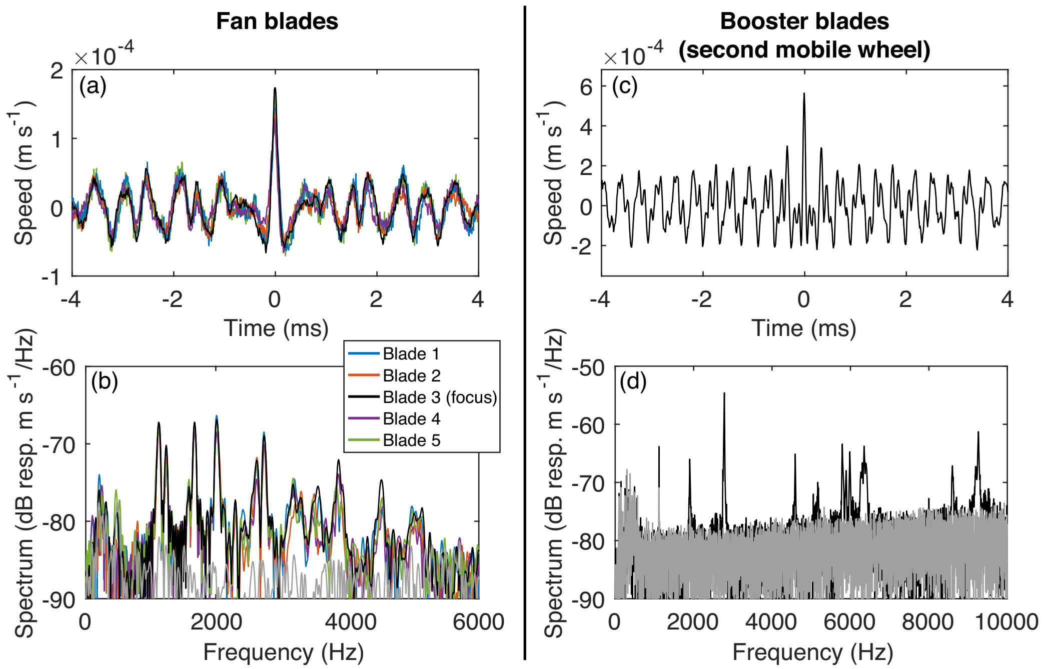


Figure 6: (a) Signal measured after TR focusing at a position of several fan blades by emitting the time-reversed impulse responses acquired at the same position on blade 3. (c) Signal measured after TR focusing on a booster blade (second mobile wheel). (b) and (d) Amplitude spectra of the signals in (a) and (c). The noise (grey) is the amplitude spectrum of a background noise signal (no loudspeaker emission) of same duration as the signals in (a) and (c).

the simplified TR operation we used for the fan blades is not possible for the booster blades. Indeed, both type of blades rotate at the same time and the booster blades are much smaller than the fan blades. Therefore, the fan blades are not at the same positions i.e., the medium between the loudspeakers and the booster blades is different, when we rotate the wheel axis to place a booster blade at the position of the previously excited blade. Consequently, the impulse responses are different and we have to record them for each booster blade inspection.

The pulse shape and the spectrum are different on the fan and booster blades but we excite about ten eigenmodes on the two types of blades. For booster blades, this is in agreement with our measurements on the similar 'small' blades in the laboratory (Fig. 2g). Because fan blades are larger, their eigenfrequencies are lower ($f < 5$ kHz) than the booster blades (1 kHz $< f <$ 10 kHz). These two blades are not rigidly clamped to their wheel, therefore we can control their eigenfrequencies independently from the rest of the wheel. We noted that the eigenfrequencies can be slightly different for blades of the same type. We discuss the implications of this observation on the uncertainty of the TR testing technique in section 5.1.

#### *3.2.2. Exciting Blades Deeper Inside the Jet Engine*

In order to check that the sound emitted by the LS can propagate through the engine and excite blades located deeper inside, we conducted TR focusing experiments with several microphones placed around the engine. The procedure is the same as described in section 2 except that we focus sound in air on the microphones. A microphone is located on the side of the engine, recording sound propagating through the engine from a hole used for endoscopy measurements (M2, Fig. 5) and two microphones are located at the opposite extremity of the engine with respect to the TRM (M3 and M4). To verify sound attenuation through the engine, one microphone (M1) is placed next to the LS. Microphones M2 and M3 are surrounded by foam to attenuate the sound coming from the exterior of the engine and to be more sensitive to the sound propagating through the engine. Pulses are measured on the four microphones and their maximum amplitude is given relatively to M1 in Table 1. The excitation amplitude decays by about 12.2 dB between the TRM and the measurement position on the side of the engine (M2). Through the whole engine, amplitude decays by about 25 dB (M3 and M4). Note that the amplitude on microphone M3, embedded in foam, is slightly lower that on microphone M4, located at the same position. It is then a priori possible to inspect blades deep inside the engine. There are however some limitations with the current setup and we discuss them in section 5.

Table 1: Excitation amplitude recorded on the four microphones with respect to microphone M1

| Microphone | M1 | M2 | M3 | M4 |
|---|---|---|---|---|
| Amplitude (dB) | 0 | -12.2 | -26.7 | -24.1 |

## 4. Detecting Damage from Eigenfrequency Shift

We now measure the variation of the eigenfrequencies of the three blades presented in section 3.1 when damage is created. Below 10 kHz, these blades have only a few narrow eigenfrequencies which can be easily distinguished. Two types of damage are created on the blades: (1) a corner of surface $S_{cut}$ is removed using a grindstone to mimic a loss of matter or (2) a slit of length $L_{slit}$ is created with a cutting device to mimic an open crack with the two sides not in contact with each other (Fig. 7ac). Because of the hardness of blade titanium, we were only able to make a slit of about 2 mm length in the small blade and our cutting device was not strong enough to cut the larger blades.

The blade resonance spectrum is recorded at several positions for each damage size. The different measurement positions are the same as on Fig. 2jkl. At a given position, it is observed that eigenfrequencies increase when the surface $S_{cut}$ of the cut corner increases and decrease when the length $L_{slit}$ of the slit increases (Fig. 7bd). Note that all eigenfrequencies are not equally sensitive to the presence of the damage (Fig. 7e). Intuitively, a slit would generally affect the frequencies of the eigenmodes with motion transverse to the direction of the slit the most. Analyzing how the eigenmodes are affected to localize a damage and assess its severity is the goal of the RUS approach [e.g. 8], but this is beyond the scope of this paper. Our proof of concept results show that damage differentiation (matter removal or slit) on a blade could be performed remotely using our method.

In average over all of the eigenmodes and all of the measurement positions on the blades, we observe that the frequency shift increases with the cut-off corner surface $S_{cut}$, for all three types of blades (Fig. 8abc). Similarly, when we create a slit along the side of the small blade, the average frequency shift decreases with the slit length $L_{slit}$ (Fig. 8e). The frequency shifts fit well with a linear law, with a $R^2$ factor close to 1 for the small and middle blades and $R^2 \simeq 0.77$ for the large blade.

These experimental results can be predicted by the Weyl theory [28]. An estimate of the number of eigenmodes $\overline{N}(f_0)$ of a thin plate below frequency $f_0$ is given by the Weyl expansion as

$$\overline{N}(f_0) = \frac{\pi(1 + (c_s/c_p)^2)S}{c_\phi^2} f_0^2 + \beta \frac{P}{2c_\phi} f_0 + o(f_0), \tag{1}$$

with $c_p$ and $c_s$ the speeds of the compressional and shear waves in the plate,

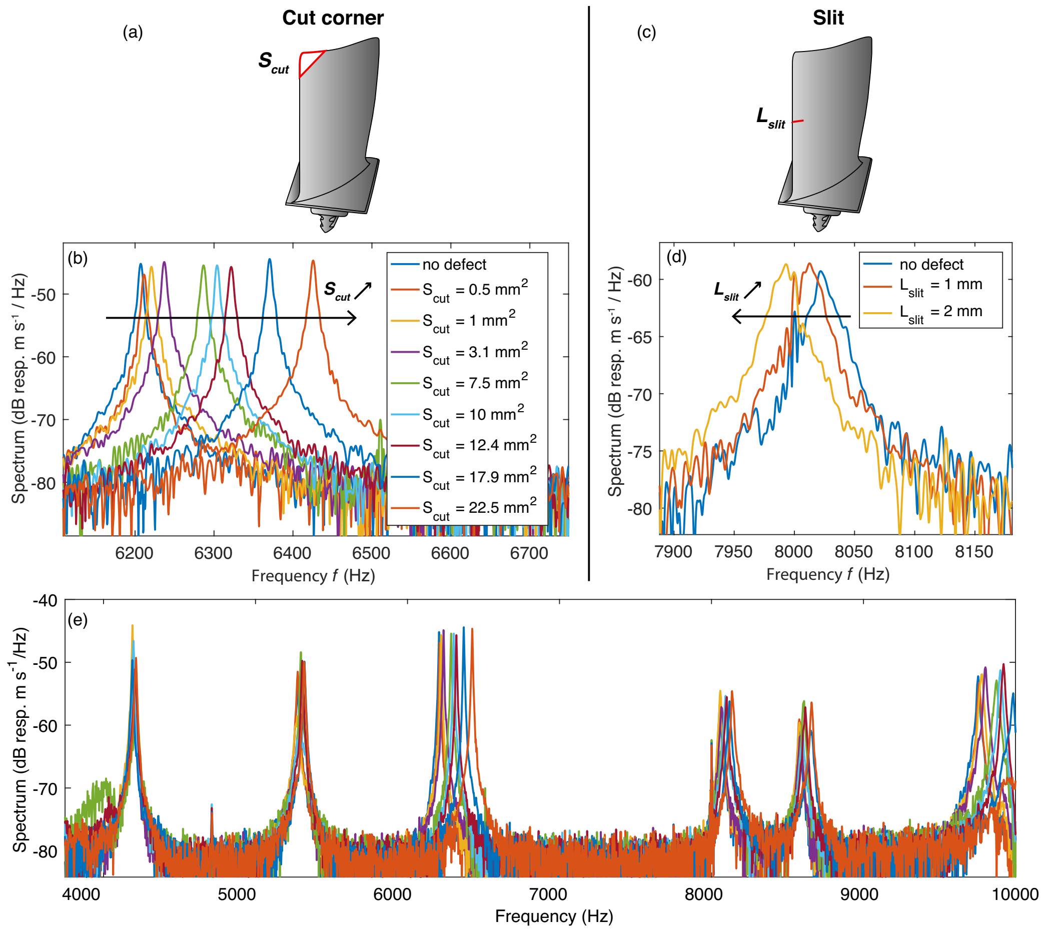


Figure 7: (a) and (c) Schematic of the damage created on the blades: (a) cut-off corner and (c) slit along the side of the blade. (b) and (d) Frequency shift of one eigenmode measured at the same position of the small blade when (b) the cut-off corner surface $S_{cut}$ increases and (d) the slit length $L_{slit}$ increases. (e) Amplitude spectra showing the frequency shift of different eigenmodes of the small blade when the surface of its cut corner increases (same legend as in panel (b)).

$c_\phi$, the phase speed, $S$ and $P$, the surface and perimeter of the plate and $\beta$, a parameter that is positive in the case of free boundary conditions. Damaging the plate modifies its surface $S$ and/or perimeter $P$ and, hence, affects the number $\overline{N}(f_0)$ of eigenmodes. For the cut-off corner, the blade surface $S$ decreases and perimeter $P$ increases. Since $\overline{N}(f_0)$ is more sensitive to changes in the surface $S$ (coefficient proportional to $f_0^2$) than to the perimeter $P$ (coefficient proportional to $f_0$), the number of eigenmodes $\overline{N}(f_0)$ decreases and the eigenfrequencies increase. In contrast, for a slit of increasing length, the surface is constant while the perimeter increases. Consequently, the number of eigenmodes $\overline{N}(f_0)$ increases and the eigenfrequencies decrease. Note that when the damage is a cut corner of surface $S_{cut}$, the average frequency shift on the three blades match well with the surface ratio $S_{cut}/S$, where $S$ is the surface of the blade (Fig. 8d). Again, we can interpret this dependence using Eq. (1): the number of eigenmodes $\overline{N}(f_0)$ is proportional to the blade surface $S$ and, by definition, is also inversely proportional to the average interval between the eigenfrequencies $\Delta f$. A variation $\delta S$ of the blade surface is then linked to a variation $\delta(\Delta f)$ of the interval between eigenfrequencies: $\frac{\delta(\Delta f)}{\Delta f} \propto \frac{\delta S}{S}$. Consequently, by measuring frequency shift with respect to a reference frequency value, one can detect a smaller damage on the small blade than on the large blade. For example, if the detection threshold of the frequency shift in 10 Hz, we can detect a damage of size 2 mm$^2$ on a small blade, 10 mm$^2$ on a medium blade and 15 mm$^2$ on a large blade.

## 5. Discussion

### *5.1. Causes of Uncertainties on Damage Detection*

Our estimate of the damage size from the shift in eigenfrequencies suffers from the same biases than other methods based on comparison with a reference measurement: any parameter affecting the reference eigenfrequencies is a possible cause of uncertainty on the damage size estimate.

An important possible cause of uncertainty is the difference of constraints applied on the blade between the reference and control measurements. To verify this, we conducted a series of experiments with a thin 1.5-mm thick duralumin plate of dimensions 10 cm by 10 cm clamped with a binder clip in front of the TRM (Fig. 9a). The clip exerts a strong stress and significantly affects the plate eigenmodes depending on its position. Indeed, the eigenfrequency measured at the same position of a plate for ten different clamping positions varies by about 2% (about 40 Hz in the case of this eigenmode) while its amplitude varies by about 120%. The large variation in the eigenmode amplitude depending on the clamping location might be explained by the fact that the vibration amplitude may be much lower when the clamping constrains an antinode of the eigenmode than when it contrains one of its node. It is then important to control the eigenfrequencies of a blade in similar stress conditions as during the reference measurements. In our laboratory experiments, the investigated blades are placed on 3D-printed supports which do not exert strong constraints on them. With these supports, the uncertainty on the eigenfrequencies is about 0.3%.

Another cause of uncertainty on the frequency shift comes from the fact that the blade eigenmodes cannot be all measured when we focus at a given measurement position. Indeed, this position can correspond to a node of some eigenmodes and to the antinode of other eigenmodes. This is the cause of the error bars on the frequency shift averaged over all measurement positions in Fig. 8. Practically, one should try to focus at the same location on the blade between the reference and monitoring measurements to evaluate the potential frequency shift for the same eigenmodes. Preferential positions to focus on the blade are its sides and corners because vibration amplitude is higher (Fig. 3).

Finally, we noted that the eigenfrequencies of blades of the same type can be different. For the three similar small blades investigated, the frequency discrepancy can be as much as 100 Hz (Fig. 9b) which is important because a shift of 10 Hz corresponds to a damage of about 2 mm$^2$ on these blades (Fig. 8a). That said, practically each individual blade of an aircraft engine are identified with a reference number during inspection. Therefore, the relevant information to assess the development of a damage on a given blade is the relative shift of its eigenfrequencies with respect to reference measurements made on the same blade and not their absolute value.

### *5.2. On site Applicability of the Time Reversal Technique*

As discussed in section 5.1, it is important for future remote inspection of blades inside a jet engine that eigenfrequency measurements are performed in similar stress conditions. In particular, the fan and booster blades we investigated are unclamped and the stress conditions on these blades are different depending on if they are located at the top (less stressed) or the bottom (more stressed) of the wheel. Therefore, they have to be located at the same position between two inspections.

The on-site experiments described in section 3.2 show that a small array composed of a few PC loudspeakers is sufficient to excite the blades in the jet engine, even though this structure is designed to attenuate vibrations. Note that a technique based on the Hadamard matrix, using all LS simultaneously to record the impulse responses, could be used to increase the signal-to-noise ratio with a given array of LS [29]. The TR technique is therefore relatively inexpensive and easy to install for routine inspection. The advantage of this technique compared to the standard coin-tap method, which is usually conducted by a human operator, is that it creates a contactless excitation and it is more reproducible because the excitation amplitude and location can be controlled more precisely.

The principal weakness of our experimental setup for on site applications is that the laser vibrometer incidence must be almost perpendicular to the investigated surface to get enough reflected light and this is difficult to achieve on curved blades embedded in the engine. For the laboratory experiments, we had to use reflecting tape on the blades. Moreover, a direct light path is necessary between the vibrometer and the scanned blade, compromising the inspection of blades deeper in the engine. Future studies could for example use a holographic interferometer, which is more suited for rough surfaces, or flexible fiber optics. Note that nondestructive evaluation during the fabrication process is less restrictive and the TR technique could be used with a laser vibrometer in this context.

## 6. Conclusions

Conventional nondestructive evaluation procedures of jet engine blades are often expensive and time consuming because the blades are difficult to access, which require partial disassembly of the engine. In this paper, we applied a nondestructive acoustic technique based on time reversal to remotely and locally evaluate the eigenfrequencies of individual blades. The technique has been applied on individual blades of different sizes and in the real context of a jet engine. Blades can be excited individually and independently of their neighbors, even when they are partially hidden by other blades and inside a reverberant cavity (hollow cylinder or the jet engine). We observed that the edges of the blades are preferential positions to perform monitoring of eigenfrequencies because their vibration displacement is higher and there are less nodal locations than at the middle of the blades. Besides, we noted that the eigenfrequencies of identical blades can be different. Therefore, damage detection should rely on the eigenfrequency shifts with respect to reference measurements made on each individual blade rather that on the absolute value of the eigenfrequencies. The blade eigenfrequencies are measured with sufficient precision to enable the detection of frequency shifts caused by millimeter size damage on the blades. Our experimental procedure uses a laser vibrometer which is not well suited for practical on-site applications because blades have a textured surface and a curved shape and it requires a direct path between the laser and the blades. However, this time reversal technique could be applied in the future using more flexible remote vibration sensors (e.g. fiber optics) to advantageously replace conventional techniques, such as the coin-tap method, for rapid, relatively inexpensive, reproducible and remote monitoring of blades or other plate-like objects during their fabrication process or their routine inspection.

## 7. Acknowledgments

This work was supported by LABEX WIFI (Laboratory of Excellence ANR-10-LABX-24) within the French Program ‘Investments for the Future’ under reference ANR-10- IDEX-0001-02 PSL. The initial manuscript was greatly improved thanks to the useful comments of two anonymous reviewers.

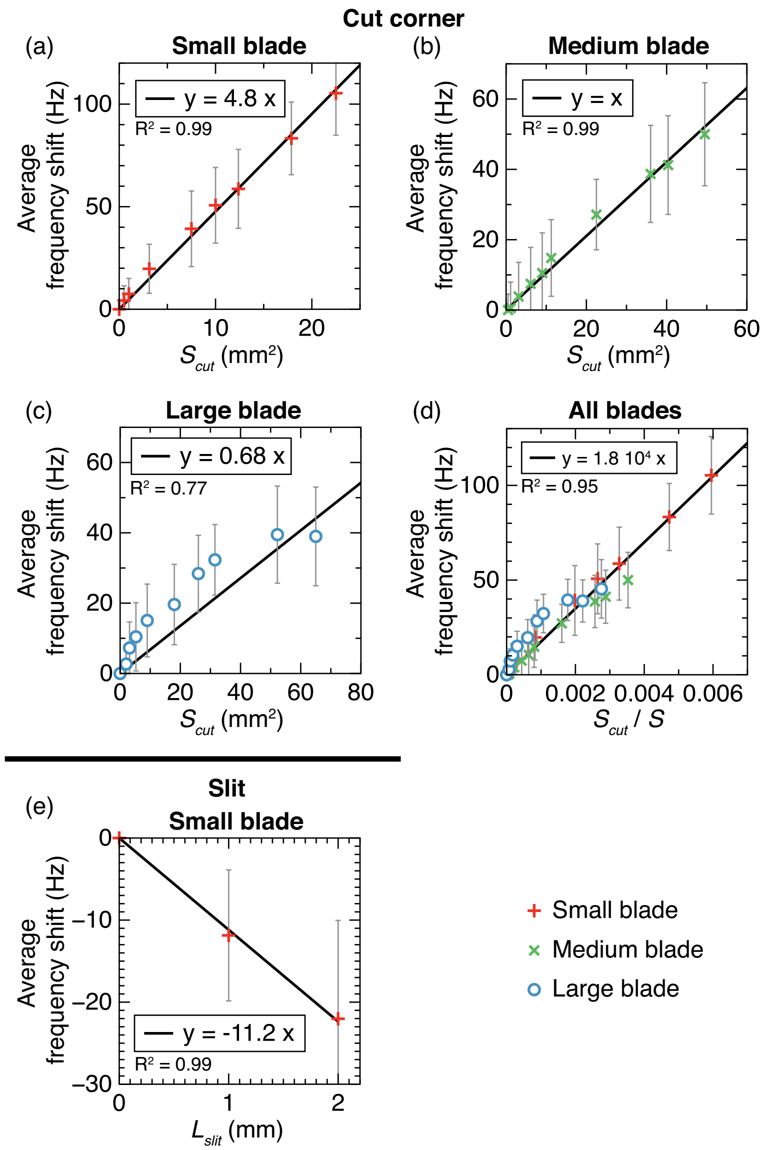


Figure 8: (a) Frequency shift averaged over all blade eigenmodes and all measurement positions as a function of the damage size. (a)-(d) Shift when a corner is cut on (a) the small blade, (b) the medium blade and (c) the large blade as a function of the surface $S_{cut}$ of the cut corner and (d) for all the blades as a function of $S_{cut}$ normalized by the blade surface $S$. (e) Frequency shift when a slit is made on the small blade as a function of the slit length $L_{slit}$. The black line in each panel represents the best linear fit to the data.

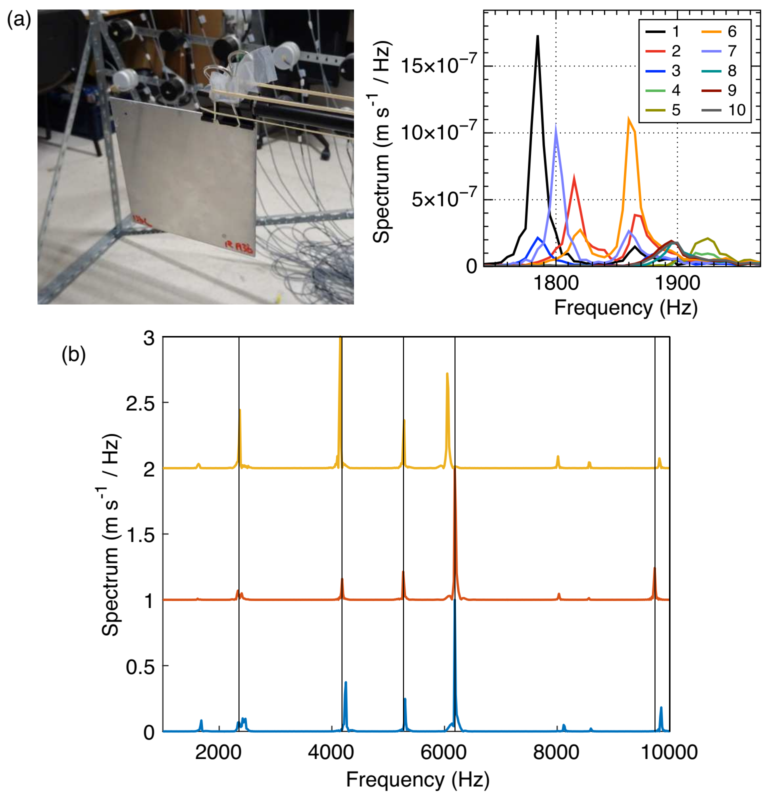


Figure 9: (a) (Left) Photograph of a duralumin plate held with a binder clip in front of the TRM. (Right) Eigenmode measured at the same position of the plate for ten different positions of the clip (different colors). (b) Comparison of the amplitude spectra of a pulse focused at the same position on three similar small blades.

[1] K. Diamanti, C. Soutis, Structural health monitoring techniques for aircraft composite structures, Progress in Aerospace Sciences 46 (2010) 342–352. doi:10.1016/j.paerosci.2010.05.001.

[2] A. Katunin, K. Dragan, M. Dziendzikowski, Damage identification in aircraft composite structures: A case study using various non-destructive testing techniques, Comp. Struct. 127 (2015) 1–9. doi:10.1016/j.compstruct.2015.02.080.

[3] I. Amenabar, A. Mendikute, A. López-Arraiza, M. Lizaranzu, J. Aurrekoetxea, Comparison and analysis of non-destructive testing techniques suitable for delamination inspection in wind turbine blades, Composites: Part B 42 (2011) 1298–1305. doi:10.1016/j.compositesb.2011.01.025.

[4] B. Park, Y.-K. An, H. Sohn, Visualization of hidden delamination and debonding in composites through noncontact laser ultrasonic scanning, Composites Science and Technology 100 (2014) 10–18. doi:10.1016/j.compscitech.2014.05.029.

[5] P. Cawley, R. Adams, The mechanics of the coin-tap method of non-destructive testing, J. Sound Vib. 122 (1988) 299–316. doi:10.1016/S0022-460X(88)80356-0.

[6] A. Migliori, T. Darling, Resonant ultrasound spectroscopy for materials studies and non-destructive testing, Ultrasonics 34 (1996) 473–476. doi:10.1016/0041-624X(95)00120-R.

[7] S. Petit, M. Duquennoy, M. Ouaftouh, F. Deneuville, M. Ourak, S. Desvaux, Non-destructive testing of ceramic balls using high frequency ultrasonic resonance spectroscopy, Ultrasonics 43 (2005) 802–810. doi:10.1016/j.ultras.2005.06.003.

[8] K. Flynn, M. Radovic, Evaluation of defects in materials using resonant ultrasound spectroscopy, J. Mater. Sci. 46 (2011) 2548–2556. doi:10.1007/s10853-010-5107-y.

[9] I. Solodov, J. Bai, G. Busse, Resonant ultrasound spectroscopy of defects: Case study of flat-bottomed holes, J. Appl. Phys. 113 (2013) 223512. doi:10.1063/1.4810926.

[10] J. Pan, Z. Zhang, J. Wu, K. Ramakrishnan, H. Singh, A novel method of vibration modes selection for improving accuracy of frequency-based damage detection, Composites Part B: Engineering 15 (2019) 437–446. doi:10.1016/j.compositeb.2018.08.134.

[11] B. Anderson, M. Remillieux, P.-Y. Le Bas, T. Ulrich, Time Reversal Techniques. Nonlinear Ultrasonic and Vibro-Acoustical Techniques for Nondestructive Evaluation, Springer, 2019. doi:10.1007/978-3-319-94476-014.

[12] S. Turkaya, R. Toussaint, F. Eriksen, M. Zecevic, G. Daniel, E. Flekkoy, J. Maloy, Bridging aero-fracture evolution with the characteristics of the acoustic emissions in a porous medium, Front. Phys.doi:10.3389/fphy.2015.00070.

[13] L. Chehami, J. de Rosny, C. Prada, E. Moulin, J. Assaad, Experimental study of passive defect localization in plates using ambient noise, IEEE transactions on ultrasonics, ferroelectrics, and frequency control 62 (2015) 1544–1553. doi:10.1109/TUFFC.2014.006935.

[14] M. Farin, C. Palerm, C. Prada, J. de Rosny, Localization of unbounded contacts on vibrating elastic plates, J. Acoust. Soc. Am. 148 (2020) 3455. doi:10.1121/10.0002778.

[15] P.-Y. Le Bas, T. Ulrich, B. Anderson, J. Esplin, A high amplitude, time reversal acoustic non-contact excitation (trance), J. Acoust. Soc. Am. 134 (2013) EL52. doi:10.1121/1.4809773.

[16] P.-Y. Le Bas, M. Remillieux, L. Pieczonka, J. Ten Cate, B. Anderson, T. Ulrich, Damage imaging in a laminated composite plate using an air-coupled time reversal mirror, Appl. Phys. Lett. 107 (2015) 184102. doi:10.1063/1.4935210.

[17] M. Farin, C. Prada, J. de Rosny, Selective Remote Excitation of Complex Structures Using Time Reversal in Audible Frequency Range, J. Acoust. Soc. Am. 146 (2019) 2510. doi:10.1121/1.5129130.

[18] M. Fink, D. Cassereau, A. Derode, C. Prada, P. Roux, M. Tanter, J.-L. Thomas, F. Wu, Time-reversed acoustics, Rep. Prog. Phys. 63 (2000) 1933–1995. doi:10.1088/0034-4885/63/12/202.

[19] C. Prada, S. Manneville, D. Spoliansky, M. Fink, Decomposition of the time reversal operator: Detection and selective focusing on two scatterers, J. Acoust. Soc. Am. 99 (1996) 2067–2076. doi:10.1121/1.415393.

[20] N. Mori, S. Biwa, T. Kusaka, Damage localization method for plates based on the time reversal of the mode-converted Lamb waves, Ultrasonics 91 (2019) 19–29. doi:10.1016/j.ultras.2018.07.007.

[21] W. Kuperman, W. Hodgkiss, H. Song, T. Akal, C. Ferla, D. Jackson, Phase conjugation in the ocean: Experimental demonstration of an acoustic time-reversal mirror, J. Acoust. Soc. Am. 103 (1998) 25–40. doi:10.1121/1.423233.

[22] G. Ribay, J. de Rosny, M. Fink, Time-Reversal of noise sources in a reverberation room, J. Acoust. Soc. Am. 117 (2005) 2866. doi:10.1121/1.1886385.

[23] C. Draeger, J. Aime, M. Fink, One-channel time-reversal in a chaotic cavities: Experimental results, J. Acoust. Soc. Am. 105 (2) (1998) 618–625. doi:10.1121/1.426252.

[24] A. Derode, P. Roux, M. Fink, Robust Acoustic Time Reversal with High-Order Multiple Scattering, Phys. Rev. Lett. 75 (23) (1995) 4207–4209. doi:10.1103/PhysRevLett.75.4206.

[25] C. Draeger, M. Fink, One-channel time reversal of elastic waves in a chaotic 2d-silicon cavity, Phys. Rev. Lett. 79 (3) (1997) 407–410. doi:10.1103/PhysRevLett.79.407.

[26] S. Yon, M. Tanter, M. Fink, Sound focusing in rooms: The time-reversal approach, J. Acoust. Soc. Am. 113 (3) (2003) 1533–1543. doi:10.1121/1.1543587.

[27] P. Dular, C. Geuzaine, F. Henrotte, W. Legros, A general environment for the treatment of discrete problems and its application to the finite element method, IEEE Transactions on Magnetics 34 (5) (1998) 3395–3398.

[28] G. Tanner, N. Sondergaard, Wave chaos in acoustics and elasticity, J. Phys. A: Math. Theor. 40 (2007) R443–R509. doi:10.1088/1751-8113/40/50/R01.

[29] C. Prada, J. de Rosny, D. Clorennec, J. Minonzio, A. Aubry, M. Fink, L. Berniere, P. Billand, S. Hibral, T. Folegot, Experimental detection and focusing in shallow water by decomposition of the time reversal operator, J. Acoust. Soc. Am. 122 (2) (2007) 761–768. doi:10.1121/1.2749442.